

VLBI Imaging of Water Maser Emission from the Nuclear Torus of NGC 1068

L. J. Greenhill

Harvard-Smithsonian Center for Astrophysics, 60 Garden St, Cambridge, MA 02138

C. R. Gwinn, R. Antonucci

Department of Physics, Broida Hall, University of California, Santa Barbara, CA 93106

and

R. Barvainis

Haystack Observatory, NEROC, Route 40, Westford, MA 01886

ABSTRACT

We have made the first VLBI synthesis images of the H₂O maser emission associated with the central engine of the Seyfert galaxy NGC 1068. Emission extends about ± 300 km s⁻¹ from the systemic velocity. Images with submilliarcsecond angular resolution show that the red-shifted emission lies along an arc to the northwest of the systemic emission. (The blue-shifted emission has not yet been imaged with VLBI.) Based on the maser velocities and the relative orientation of the known radio jet, we propose that the maser emission arises on the surface of a nearly edge-on torus, where physical conditions are conducive to maser action. The visible part of the torus is axially thick, with comparable height and radius. The velocity field indicates sub-Keplerian differential rotation around a central mass of $\sim 1 \times 10^7$ M_⊙ that lies within a cylindrical radius of about 0.65 pc. The estimated luminosity of the central engine is about 0.5 of the Eddington limit. There is no detectable compact radio continuum emission near the proposed center of the torus ($T_B < 5 \times 10^6$ K on size scales of ~ 0.1 pc), so that the observed flat-spectrum core cannot be direct self-absorbed synchrotron radiation.

Subject headings: galaxies: individual, NGC 1068 — galaxies: kinematics and dynamics — galaxies: nuclei — masers

1. Introduction

The galaxy NGC 1068 is widely believed to harbor a Seyfert I nucleus that is obscured by a dusty edge-on torus (Antonucci 1993, and references therein). X-rays of energies up to 10 keV from the central engine of the active galactic nucleus (AGN) are blocked by an atomic column density of at least 10²⁵ cm⁻² (Mulchaey et al., 1992). The inferred axis of the torus is nearly north-south,

and broadline optical and ultraviolet emission is scattered into the line of sight on angular scales as small as 0''.1 (Antonucci & Miller 1985, Antonucci, Hurt, & Miller 1994, Capetti et al., 1995). An ionization cone is visible in [OIII] light (Evans et al., 1991, Macchetto et al., 1994) and is closely associated with a roughly north-south radio jet (Ulvestad et al., 1987, Muxlow et al., 1996). A jet component near the southern end, at the base of the cone has a rising spectrum, suggesting that the central engine lies approximately there (Gallimore et al., 1996a), as ultraviolet polarization measurements also indicate (Antonucci, Hurt, & Miller 1994, Capetti et al., 1995).

A water maser source (Claussen, Heiligman, & Lo 1984) lies at the suggested location of the central engine (Claussen & Lo 1986, Gallimore et al., 1996b). Claussen & Lo (1986) showed that the H₂O maser is compact on parsec scales and first suggested that the dusty molecular torus of the AGN is responsible for the maser emission. Thus, the structure and velocity field of the torus might be traced by the maser, which can be studied with Very Long Baseline Interferometry (VLBI) on scales as small as 0.1 milliarcseconds (mas), despite high foreground column densities. At a distance of 15 Mpc, 0.007 pc subtends 0.1 mas. The H₂O maser emission marks the presence of warm (~ 400 K), high density ($n_{\text{H}_2} \sim 10^8 - 10^{10} \text{ cm}^{-3}$) molecular gas (Elitzur 1992). The line-of-sight velocity field also must be coherent (with respect to the sound speed) on size scales $\gg 10^{13} \text{ cm}$ to achieve significant amplification (Reid & Moran 1988). The maser emission extends about $\pm 300 \text{ km s}^{-1}$ from the galactic systemic velocity of 1150 km s^{-1} adopted by Gallimore et al., (1996b). (Velocities throughout are heliocentric and assume the optical astronomical definition of Doppler shift.) Gallimore et al., (1996b) used the Very Large Array (VLA) of the NRAO¹ to partially resolve the source structure on scales of 40 mas, or about one

The National Radio Astronomy Observatory is operated by Associated Universities, Inc, under cooperative agreement with the National Science Foundation.

third of the synthesized beamwidth, and inferred that the maser traces the midplane of the nuclear torus. Preliminary VLBI measurements also detected a position-velocity gradient in the maser on angular scales of 0.4 mas (Gwinn et al., 1993). We present the first VLBI synthesis images of the maser emission at and redward of the systemic velocity.

2. Observations and data

We observed the H₂O maser emission in NGC 1068 for about 8 hours on 1994 November 5 with the Very Long Baseline Array (VLBA), and the VLA operating as a phased 132 m aperture. The sensitivity of the VLA was critical to the observations because of the low peak flux density of the maser, ~ 0.6 Jy. We recorded bandpasses tuned to bandcenter heliocentric velocities of 1438.11, 1342.17, and $1165.80 \text{ km s}^{-1}$. The velocity range 1210 to 1285 km s^{-1} was not observed.

Figure 1 shows the velocity coverage of the observations in the context of the maser spectrum. The channel spacing in each band was 0.45 km s^{-1} . We tracked variations in atmospheric phase using the maser feature at 1462 km s^{-1} as a reference and subtracted them from the data for other features.

Calibration and imaging relied upon standard spectral-line VLBI techniques. We fit a 2-D Gaussian model to the brightness distribution of every statistically significant peak in the images for each velocity channel. The centroid positions, measured with respect to the reference, are sensitive to calibration errors caused by uncertainties in the station clocks and positions, earth orientation parameters, and astrometric maser position. Only uncertainties in the last two items are significant. These cause position errors that are linearly proportional to the velocity offset from the reference. For the emission at 1325 km s^{-1} and 1135 km s^{-1} , the errors are $\lesssim 50 \mu\text{as}$ and $\lesssim 100 \mu\text{as}$, respectively.

3. Spectral-line images

Five dominant clumps of maser emission are distributed almost linearly on the sky, with pronounced velocity gradients (Figure 2). The emission close to the systemic velocity (hereafter “systemic emission”) is extended roughly east-west and lies to the southeast of the red-shifted emission. It displays a velocity gradient of about $50 \text{ km s}^{-1} \text{ mas}^{-1}$, with the higher velocity emission in the west (Figure 3). The emission between about 1315 and 1465 km s^{-1} (hereafter “red-shifted emission”) is distributed roughly in an arc about 0.6 pc long, at a position angle of about -45° . The red-shifted emission is separable into clumps whose velocities and velocity spreads increase with decreasing separation from the systemic emission. Clump 4, which lies closest to the systemic emission, has the greatest velocity spread ($\sim 100 \text{ km s}^{-1}$) but a reduced average velocity. The uncertainties in measured positions after the data calibration are typically 100 times less than the characteristic size scale of the maser source. The 0.4 mas gradient reported earlier by Gwinn et al., (1993), along a position angle of 75° (note correction of earlier typographical error), between 1391 and 1415 km s^{-1} , is consistent with the current observations.

No radio continuum emission was detected in our observations. An average of all spectral channels redward of 1290 km s^{-1} shows no statistically significant emission other than that which is related to the maser. The limiting flux density is 0.45 mJy (1σ), corresponding to a brightness temperature of $< 5 \times 10^6 \text{ K}$ for a tapered beamwidth of $1.4 \times 1.0 \text{ mas}$. (We note that continuum emission coincident with clumps 1 – 4 is only excluded at the 0.8 mJy level.)

4. The molecular torus and the central engine

We propose that the observed red-shifted maser emission traces part of the limb of an edge-on rotating torus, rather than the midplane (cf. Gallimore et al., 1996b). This torus is thick in both

radial and axial directions and has an opening angle on the order of 90° . Along the limb, the orbital motion is parallel to the line of sight, and produces a substantial amplification along a velocity-coherent path. Where the motion is transverse to the line of sight, the limited thickness of the maser layer precludes significant amplification except near the equatorial plane, where maser emission is perhaps visible perhaps because it amplifies the 22 GHz continuum flux associated with the central engine or radio jet. Observations that support this model are 1) the position angle of the red-shifted emission relative to the radio jet axis; 2) a falling rotation curve for cylindrical radii beyond ~ 0.4 pc; 3) the position-velocity gradient of the systemic maser features; and 4) the location of red-shifted maser emission, observed by us, with respect to the blue-shifted emission, observed by Gallimore et al., (1996b). (The cylindrical radius is defined with respect to an axis passing through the maser emission that lies at the adopted systemic velocity, with a position angle of approximately 0° (Antonucci, Hurt, & Miller 1994; Gallimore et al., 1996a).)

The model in Figure 4 shows the observed emission and the proposed location of the blue-shifted emission. In the VLA map of the maser (Gallimore et al., 1996b) the weighted average centroid of the blue-shifted emission between 800 and 850 km s^{-1} lies 42 mas due east of the red-shifted emission at about 1425 km s^{-1} , with 8 mas formal uncertainty in right ascension and declination. Based on this and the intrinsic symmetry of an edge-on torus, we hypothetically reflect the red emission in velocity about the systemic velocity and in space about the axis of the torus to obtain a “V”-shaped structure.

A thick torus requires vertical support, possibly from internal velocities, radiation forces, or magnetic fields. The ratio of internal motions to orbital velocity, v_i/v_ϕ , is approximately equal to the ratio of height to radius, h/R (Krolik & Begelman 1988). The requisite velocity v_i is on the order of 100 km s^{-1} , corresponding to temperatures at which molecular gas could not survive if the motions were thermal. However, the spread of velocities in clumps 1 – 4 approaches 100 km s^{-1} . The source of the supersonic turbulence is unclear, although our data show that internal motions increase dramatically close to the central engine, suggesting that it could drive these motions. Pier & Krolik (1992) show that radiation forces acting on dust grains close to the inner radius may be comparable to gravitational forces. As well, gas densities of 10^{10} cm^{-3} and magnetic field strengths of a few Gauss result in equipartition of rotational and magnetic energy. Emmering, Blandford, & Shlosman (1992) and Königl & Kartje (1994) model centrifugally-driven flows from thin magnetized accretion disks. At sufficiently large radii the flow may be dusty, which is favorable to maser emission, though the model molecular gas density is too small.

The maser emission may arise from clouds that move in a warmer or more turbulent medium. Amplification occurs in gas with thermal motions of less than a few km s^{-1} but the turbulent velocities of the red-shifted emission are at least an order of magnitude greater. The maser clouds may be the inward extension of a system of molecular cloud cores that lie close to the galactic plane at radii of at least 30 pc, with turbulent velocities of ~ 100 km s^{-1} (Tacconi et al., 1994; see also Jackson et al., 1993), although the maser torus is misaligned with respect to the galactic plane by approximately 65° .

The minimum radius at which maser emission is observed, ~ 0.4 pc, is close to the radius at which dust sublimates (Barvainis 1987; Laor & Draine 1993). Graphite grains smaller than $0.05 \mu\text{m}$ sublimate within a radius of $r_{\text{sub}} \sim 0.4L_{45}^{0.5}$ pc, where L_{45} is ultraviolet luminosity in units of 10^{45} ergs s^{-1} (Barvainis 1987). Most of the intrinsic bolometric luminosity is radiated at ultraviolet wavelengths. Hence, we adopt $L_{45} = 0.6$ (Pier et al., 1994), for which $r_{\text{sub}} \sim 0.4$ pc. Pier & Krolik (1993) find the model infrared spectrum of a dusty torus best fits the observed spectrum of NGC 1068 for a 0.5 pc inner radius and 800 K effective temperature, somewhat less than the sublimation temperature of silicate dust. The agreement of r_{sub} with the maser observations may be related to the important role that dust can play in the thermodynamics of the maser pump cycle (e.g., Collison & Watson 1995) and in obscuring the nuclear continuum. Ablation of the component clouds of the torus by photons from the central engine (Krolik & Begelman 1986, 1988; Pier & Voit 1995) also fixes the inner radius to be on the order of 1 pc.

The radial extent of maser emission is probably governed by limitations in the maser excitation mechanism operating in the torus clouds. Emission can be driven by wind or jet-induced shocks (Elitzur, Hollenbach, & McKee 1989, Kaufman & Neufeld 1996), or by collisional heating associated with X-ray illumination by the central engine, as proposed for NGC 4258 and NGC 1068 (Neufeld, Maloney, & Conger 1994). Both mechanisms excite only a thin layer of material. As well, curvature of the torus may block direct mechanical interaction or X-ray illumination at large radii.

The maser torus model suggests that there should be red-shifted emission visible from the southern half of the torus and systemic emission superposed along some length of the jet. The absence of southern emission may be related to the absence of strong southern jet emission, on scales smaller than about 10 pc (e.g., Ulvestad et al., 1987). Alternatively, southern radio emission may be preferentially obscured, especially if the torus is not strictly edge-on. The presence of systemic maser emission near the equator alone is consistent with the jet having a steep spectrum and a rapid decline with radius of the frequency at which it becomes optically thin. In NGC 4258, the 22 GHz jet emission is localized to radii on the order 0.2 mas scaled to a distance of 15 Mpc (Herrnstein et al., 1996). Since background continuum emission has not been observed directly by us, the relatively flat-spectrum nuclear source seen on angular scales of $\sim 0.^{\prime\prime}1$ (Gallimore et al., 1996a; Muxlow et al., 1996) cannot be entirely a self-absorbed synchrotron source. The emission is not limited to a point source; it could represent thermal emission or possibly Thompson-scattered radiation (Gallimore et al., 1996a). Background amplification may still give rise to the systemic maser features because they are relatively weak. The limit on continuum strength implies the gain is at least 40, which is modest.

From the rotation curve in Figure 3, we estimate the total mass enclosed within a radius of 0.65 pc is $\sim 1 \times 10^7 M_{\odot}$, assuming a circular orbital velocity of $\sim 250 \text{ km s}^{-1}$. The luminosity of the central engine (Pier et al., 1994) is ~ 0.5 times the corresponding Eddington luminosity. The mass is less than the approximately $2 \times 10^8 M_{\odot}$ implied by the motions of the molecular cloud cores beyond a radius of 30 pc (Tacconi et al., 1994). From VLA observations of the maser

Gallimore et al., (1996b) estimate a mass of $3 \times 10^7 M_{\odot}$ (scaled to 15 Mpc), though the VLBA observations provide a more accurate determination of the rotation curve. The VLBA mass estimate is uncertain by factors of order unity because the best-fit rotation curve is sub-Keplerian, $v \propto R^{-0.31 \pm 0.02}$ for $0.65 > R > 0.40$ pc. Self-gravity of the torus or substantial nearby stellar mass could be responsible. Alternatively, outwardly directed radiation pressure may reduce orbital velocities close to the inner edge of the torus (Pier & Krolik 1992). This proposed force and the known dispersion in maser velocities is smallest for 0.65 pc radius, at which we estimate the central mass.

If the *systemic* masers are restricted to the inner surface of the torus, then the systemic emission arises over a narrow range of radii. The changing line-of-sight projection of the orbital velocity causes a gradient in line-of-sight velocity (as a function of impact parameter in the equatorial plane), $\partial V / \partial b = 0.3 M_6^{0.5} r_{\text{pc}}^{-1.5} D_{\text{Mpc}} \text{ km s}^{-1} \text{ mas}^{-1}$, where M_6 is the central mass in units of $10^6 M_{\odot}$, r_{pc} is the radius in parsecs, and D_{Mpc} is the distance in Mpc. For parameters estimated previously from the red-shifted emission, $M_6 = 10$, $r_{\text{pc}} = 0.4$, and $D_{\text{Mpc}} = 15$, we predict a gradient of $60 \text{ km s}^{-1} \text{ mas}^{-1}$, in reasonable agreement with observation (Figure 3). Greenhill et al., (1995b) apply similar arguments to the maser disk in NGC 4258. This interpretation of the systemic emission would be bolstered if the line-of-sight velocities of individual systemic maser features are observed to drift in time, corresponding to the line-of-sight centripetal acceleration while the red and blue-shifted maser features remain fixed (cf., Greenhill et al., 1995a, Nakai et al., 1995 for NGC 4258). The large velocity dispersion of the innermost maser clump (no. 4) may in part reflect a turnover in the rotation curve, rather than just high internal motions. The turnover would correspond to the reduced line-of-sight projections of the orbital velocity of masers that lie near the inner edge of the torus and out of the sky plane that contains the red-shifted emission.

5. Summary

We have mapped the brightness distribution of H₂O maser emission at and redward of the systemic velocity in the Seyfert nucleus of NGC 1068, with sub-milliarcsecond resolution. The linear structure of the maser is misaligned with respect to the axes of the radio synchrotron jet and associated optical ionization cone. The observed maser emission can be reflected about the systemic velocity and jet axis to yield a “V”-shaped structure on the sky, and this may be interpreted as tracing the limb of a thick torus. Observations of the blue-shifted maser emission, with lower angular resolution, are consistent with this interpretation. Velocity dispersions up to $\sim 100 \text{ km s}^{-1}$ may indicate that the torus probably consists of individual maser clouds immersed in a warmer more turbulent medium.

The enclosed mass within a radius of 0.65 pc is $\sim 1 \times 10^7 M_{\odot}$, and the rotation curve is sub-Keplerian. The estimated mass is consistent with a position-velocity gradient in the systemic maser emission if the systemic emission arises on the inner edge of the torus at a radius of 0.4 pc.

For this mass, the central engine of NGC 1068 radiates about 0.5 times its Eddington luminosity. No radio continuum source was detected toward the center of the torus, which argues that the flat-spectrum continuum emission observed on larger scales is not the byproduct of a self-absorbed synchrotron source.

We are grateful to O. Blaes, J. Gallimore, and J. Krolik for helpful comments and discussions. M. Eubanks and J. R. Herrnstein provided antenna positions. We thank P. Diamond and J. Benson for assistance with an early version of the correlator model. This work was supported in part by the National Science Foundation (AST92-17784).

REFERENCES

Antonucci, R. R. J. 1993, *ARA&A*, 31, 473

Antonucci, R. R. J., Hurt, T., & Miller, J. S. 1994, *ApJ*, 430, 210

Antonucci, R. R. J. & Miller, J. S. 1985, *ApJ*, 297, 476

Barvainis, R. 1987, *ApJ*, 320, 537

Capetti, A., Macchetto, F., Axon, D. J., Sparks, W. B., & Boksenberg, A. 1995, *ApJ*, 452, L87

Claussen, M. J., Heiligman, G. M., & Lo, K.-Y. 1984, *Nature*, 310, 298

Claussen, M. J., & Lo, K.-Y. 1986, *ApJ*, 308, 592

Collison, A. J., & Watson, W. D. 1995, *ApJ*, 452, 103

Elitzur, M. 1992, “Astronomical Masers,” (Dordrecht: Kluwer), 262ff

Elitzur, M., Hollenbach, D. J., & McKee, C. F. 1989, *ApJ*, 346, 983

Emmering, R. T., Blandford, R. D., & Shlosman, I. 1992, *ApJ*, 385, 460

Evans, I. N., Ford, H. C., Kinney, A. L., Antonucci, R. R. J., Armus, L., & Caganoff, S. 1991, *ApJ*, 369, L27

Gallimore, J. F., Baum, S. A., & O’Dea, C. P. 1996a, *ApJ*, 464, 198

Gallimore, J. F., Baum, S. A., O’Dea, C. P., Brinks, E., & Pedlar, A. 1996b, *ApJ*, 462, 740

Greenhill, L. J., Henkel, C., Becker, R., Wilson, T. L., and Wouterloot, J. G. A. 1995a, *A&A*, 304, 21

Greenhill, L. J., Jiang, D. R., Moran, J. M., Reid, M. J., Lo, K.-Y., & Claussen, M. J., *ApJ*, 440, 619

Gwinn, C. R., Antonucci, R. R. J., Barvainis, R., Ulvestad, J., & Neff, S. 1993, in “Sub-arcsecond Radio Astronomy,” eds. R.J. Davis & R.S. Booth (Cambridge: Cambridge Univ. Press), 331

Herrnstein, J. R., Moran, J. M., Greenhill, L. J., Diamond, P. J., Miyoshi, M., Nakai, N., & Inoue, M. 1996, *ApJ*, in preparation

Jackson, J. M., Paglione, T. A. D., Ishizuki, S., & Rieu, Nguyen-Q 1993, *ApJ*, 418, L13

Kaufman, M. J., and Neufeld, D. A. 1996, *ApJ*, 456, 250

Königl, A., & Kartje, J. F. 1994, *ApJ*, 434, 446

Krolik, J. H., & Begelman, M. C. 1986, *ApJ*, 308, L55

Krolik, J. H., & Begelman, M. C. 1988, *ApJ*, 329, 702

Laor, A., & Draine, B. T. 1993, *ApJ*, 402, 441

Macchetto, F., Capetti, S. , Sparks, W. B., Axon, D. J., Boksenberg, A. 1994, *ApJ*, 435, L15

Mulchaey, J. S., Mushotzky, R. F., & Weaver, K. A. 1992, *ApJ*, 390, 69

Muxlow, T. W. B., Pedlar, A., Holloway, A., Gallimore, J. F., & Antonucci, R. R. J. 1996, *MNRAS*, 278, 854

Nakai, N., Inoue, M., Miyazawa, K., Miyoshi, M., & Hall, P. 1995, *PASJ*, 47, 771

Neufeld, D. A., Maloney, P. R., & Conger, S. 1994, *ApJ*, 436, L127

Pier, E. A., Antonucci, R. R. J., Hurt, T., Kriss, G., & Krolik, J. 1994, *ApJ*, 428, 124

Pier, E. A., & Krolik, J. H. 1992, *ApJ*, 401, 99

Pier, E. A., & Krolik, J. H. 1993, *ApJ*, 418, 673

Pier, E. A., & Voit, G. M. 1995, *ApJ*, 450, 637

Reid, M. J., & Moran, J. M. 1988, in “Galactic and Extragalactic Radio Astronomy, 2nd ed.,” eds. G. L. Verschuur, & K. I. Kellermann, (Berlin: Springer), ch. 6

Tacconi, L. J., Genzel, R., Blietz, M., Cameron, M., Harris, A. I., & Madden, S. 1994, *ApJ*, 426, L77

Ulvestad, J. S., Neff, S. G., & Wilson, A. S. 1987, *AJ*, 93, 22

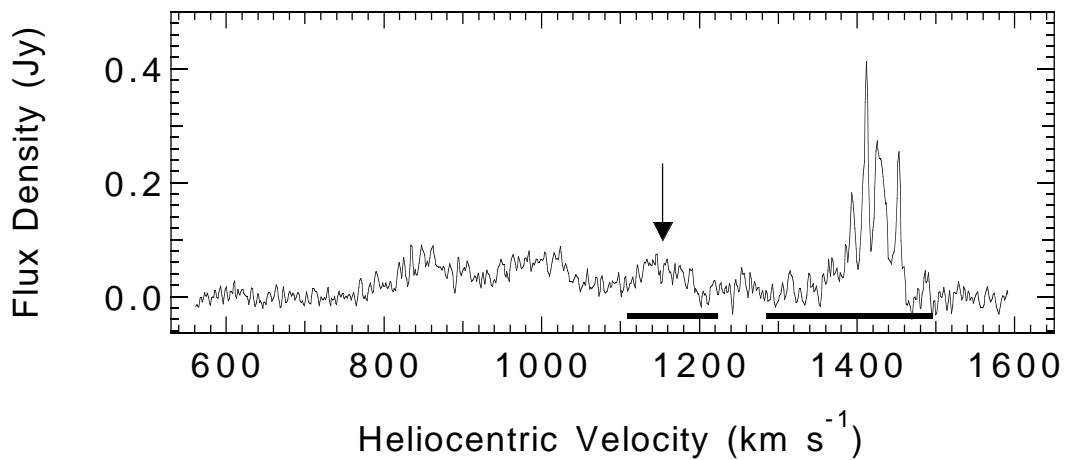


Fig. 1.— Spectrum of the H₂O maser in the nucleus of NGC 1068, taken with the Effelsberg 100-m antenna in 1993 February. The flux density calibration is accurate to about 30%. The arrow indicates the systemic velocity of the galaxy. Solid bars indicate the ranges of velocities we observed.

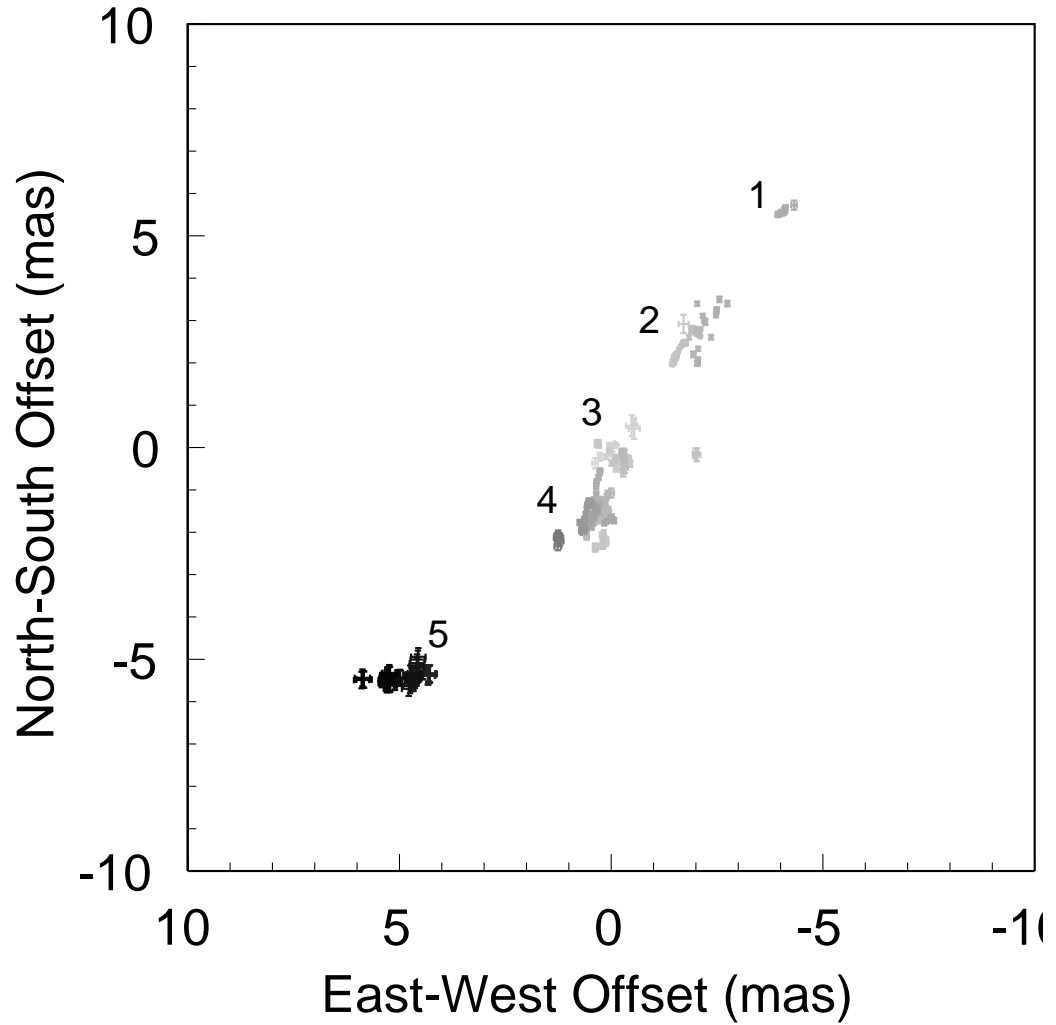


Fig. 2.— Map of the brightness distribution of the maser emission. The positions are relative to the emission at 1462 km s^{-1} and velocities are indicated by gray scale such that more red-shifted velocities are lighter. Error bars include both random and systematic measurement errors for each emission component in each spectral channel. The southeastern complex (no. 5), elongated east-west, is the emission within about 10 km s^{-1} of the systemic velocity. The rest of the emission is distributed along a position angle of about -45° and is red-shifted by $150\text{--}300 \text{ km s}^{-1}$. The blue-shifted emission between about 800 and 1100 km s^{-1} was not observed.

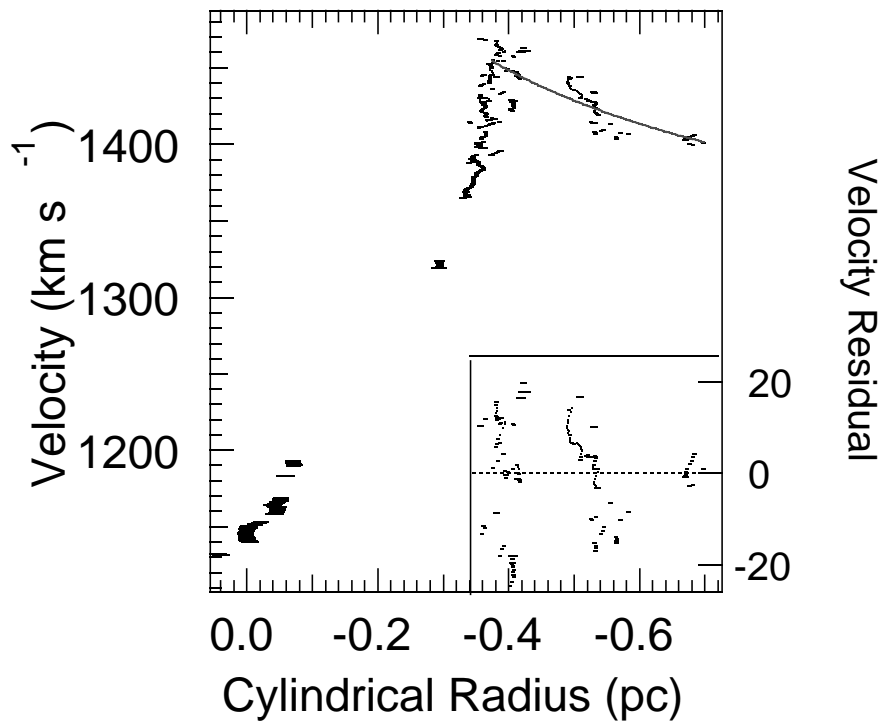


Fig. 3.— Position-velocity diagram of the maser emission. The cylindrical radius is measured with respect to the maser feature at the systemic velocity along a position angle of 90° . Error bars indicate both random and systematic measurement errors. The dashed rotation curve is discussed in section 4. (*insert*) Residuals from the fitted curve.

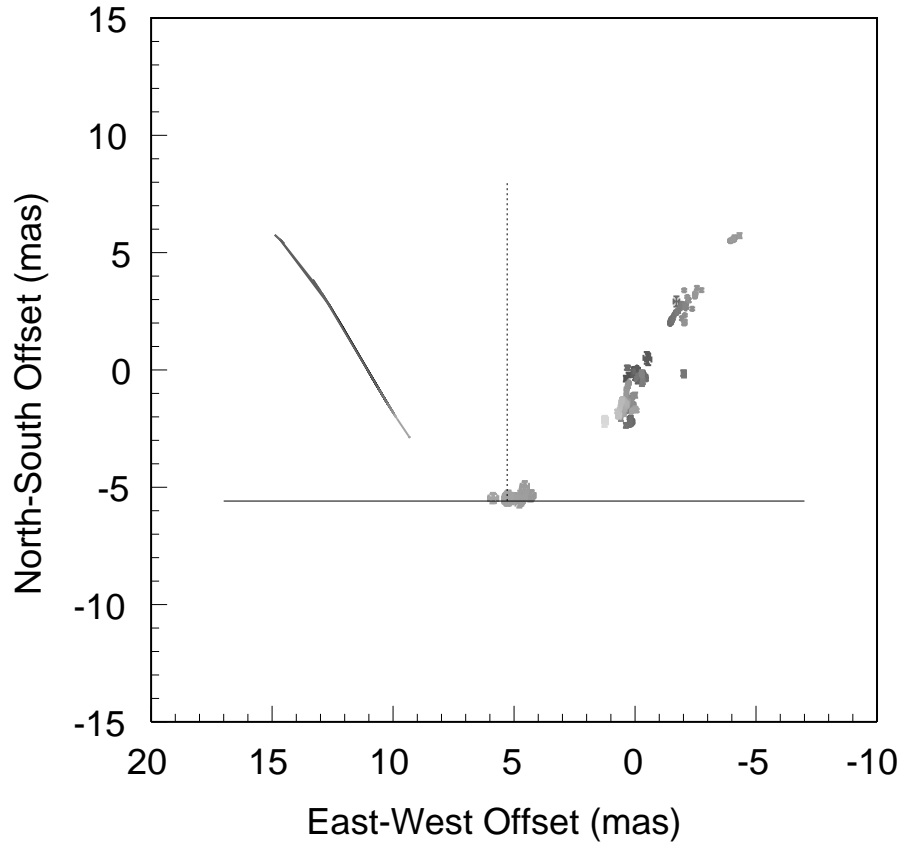


Fig. 4.— Model showing the location of the observed maser emission, as in Figure 2, and the anticipated location of the emission blue-shifted with respect to the systemic velocity. Color indicates line-of-sight velocity. The vertical line indicates the axis of the radio jet. The maser emission traces the limb of the upper half of an axially thick torus for radii between about 0.4 and 0.65 pc.